Multiperiodicity in plasmonic multilayers: General description and diversity of topologies

Alexey A. Orlov,[1] Anastasia K. Krylova,[1] Sergei V. Zhukovsky,[2,1] Viktoriia E. Babicheva,[1,2] and Pavel A. Belov[1]
[1]*ITMO University 197101, Kronverksky pr. 49, St. Petersburg, Russian Federation*
[2]*DTU Fotonik–Department of Photonics Engineering, Technical University of Denmark, Ørsteds Pl. 343, DK-2800 Kongens Lyngby, Denmark*
(Received 5 May 2014; published 10 July 2014)

We introduce multiperiodicity in periodic metal-dielectric multilayers by stacking more than two types of metal and/or dielectric layers into the unit cell. A simple way to characterize arbitrary multiperiodic multilayers using permutation vectors is suggested and employed. Effects of multiperiodicity up to its fourth order are investigated. We demonstrate that various topologies of multiple-sheet isofrequency and dispersion surfaces exist for such plasmonic multilayers, including a photonic realization of nontrivial isolated Dirac cones.

DOI: 10.1103/PhysRevA.90.013812 PACS number(s): 42.70.Qs, 78.67.Pt, 02.10.Ox, 02.10.Yn

I. INTRODUCTION

Stratified media are a very well-known object in physics [1–4] which is still revealing new and unique properties [5–7]. Efforts of recent years in the fabrication of nanostructured layered media demonstrate properties able to surpass those of natural materials. So-called metamaterials are one of the best examples of rapid progress in the field of research of artificial media. Metal-dielectric multilayered optical metamaterials, plasmonic multilayers [8], possess a variety of striking electromagnetic phenomena that include broadband all-angle negative refraction [9,10], anomalous birefringence [11,12], k-dependent precession of the optical axis [13], and ultrahigh values for the Purcell factor [14,15].

Electromagnetic response of periodic layered metal-dielectric nanostructures is the subject of many theoretical [16,17] and experimental [18,19] investigations. In such multilayers, the layer thicknesses (the characteristic size of a unit cell) are typically much smaller than the wavelength of light that interacts with the multilayer. Therefore, it is commonly assumed that the effective-medium approximation holds, so one can say that the multilayer exhibits some sort of an effective response attributable to the entire medium rather than to the individual layers. Recently, it was found out that this assumption is not necessarily true, as the wavelength of certain modes that can propagate in some plasmonic multilayers, notably hyperbolic metamaterials (HMMs), can be orders of magnitude smaller that the vacuum wavelength of light, breaking the effective-medium limit even for nanometer-scale layers [20,21]. However, it was also shown that it is still possible to build an effective-medium model with a nonlocal nature [22].

When the local effective-medium model ceases to be applicable (either by virtue of photonic band-gap effects [20] or by virtue of optical nonlocality [22]), the effects related to the composition of the unit cell start to play a significant role in the optical properties of a periodic plasmonic multilayer. This has recently opened up an exciting emerging area of study related to plasmonic multilayers where layers are arranged in a more complex fashion than just alternating the same metal and dielectric layers over and over. Two recent examples of such structures, namely, multiscale HMMs [23] and photonic hypercrystals [24], have shown a variety of interesting effects potentially of use for hyperlensing and light-matter interaction control.

Among other things, it was shown that the metamaterial's optical response in wave-vector space becomes increasingly more complex as the number of layers in the unit cell grows [23]. Therefore, a systematic study of such metamaterials is warranted. In this paper, we focus on *multiperiodic* plasmonic metamaterials, which are periodic metal-dielectric multilayers with the unit cell consisting of more than two layers. Specifically, by incorporating several different metals and/or dielectrics in the unit cell, we require that more than one kind of plasmonic interfaces are present in the metamaterial. We investigate the effects brought about by this added complexity, and show that propagating bulk plasmonic waves form isofrequency surfaces with multiple-sheet topology in the k-space, along with other interesting features such as the Dirac-type cones.

The paper is organized as follows. In Sec. II, we introduce the basic concept of multiperiodicity in metal-dielectric multilayers. In Sec. III, we develop a transfer-matrix approach to multiperiodic multilayers, using permutation vectors to make it applicable to multilayers with different layer arrangement in a unit cell. Section IV follows with the derivation of the dispersion equations for these multilayers, and Sec. V analyzes these equations in the long-wavelength limit. In Sec. VI, we explore the band structure of multiperiodic multilayers. Finally, Sec. VII summarizes the paper.

II. MULTIPERIODICITY IN MULTILAYERS

One needs at least two different layers to form a periodic multilayered structure. For plasmonic multilayer, these layers are dielectric and metal ones. This means that in order to form a plasmonic multilayer we need no fewer than one metal-dielectric (plasmonic) interface, which is always present between, a dielectric and a metal layer. The basic case of a single plasmonic interface in the unit cell, corresponding to the ordinary periodic metal-dielectric plasmonic multilayers, has been considered widely in the literature [8].

Multiperiodicity assumes that there are two or more different kinds of plasmonic interfaces in the structure. In what follows, we will consider mainly (but not exclusively) multiperiodicity of the second order: biperiodicity. To this end, we double the number of layers in the period in comparison with the basic case, and choose materials in such a way as to

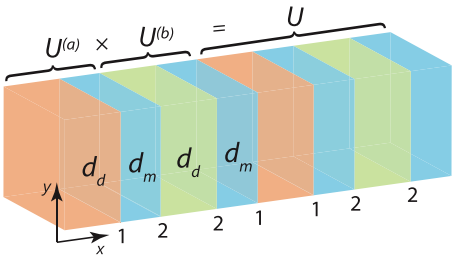

FIG. 1. (Color online) Diagram of a multiperiodic multilayer formation by means of $U^{(a)}$ and $U^{(b)}$. Layers of different materials are marked with different colors, with 1 and 2 denoting plasmonic interfaces of two kinds. Period of the structure is $\mathfrak{d} = 2(d_d + d_m)$.

have two nonequivalent kinds of plasmonic interfaces in the resulting structure.

Consider the unit cell U composed of two two-layered basic unit cells $U^{(a)}, U^{(b)}$ as shown in Fig. 1. In these terms, multiperiodicity requires $U^{(a)} \neq U^{(b)}$. Given the layer materials set $\{D^{(1)}, D^{(2)}, M^{(1)}, M^{(2)}\}$ with two dielectrics and two metals (Fig. 2), there are $P_2^4 = 4!/2! = 12$ partial permutations of how we can order layers in the basic biperiodic unit cell. Since the structure is periodic and infinite, it is invariant under the shift S or inverse I operators applied to U. Therefore, it does not matter how we arrange basic unit cells in U, i.e., $U = U^{(a)}U^{(b)}$ is identically equal to $U = U^{(b)}U^{(a)}$ as $S^2\{U^{(a)}U^{(b)}\} = U^{(b)}U^{(a)}$, so the structure is invariant to simultaneous inverse of layer order $I\{U^{(a)}\}I\{U^{(b)}\}$ in $U^{(a)}, U^{(b)}$ as well since $S^2\{I\{U^{(a)}\}I\{U^{(b)}\}\} = I\{U^{(a)}U^{(b)}\}$, i.e., identical to $U = U^{(a)}U^{(b)}$.

As was stated above, U in the case of plasmonic multilayers should be composed of alternating metal and dielectric layers. We will also require that no additional sort of plasmonic interface may arise when $U^{(a)}$ is stacked with $U^{(b)}$. Basically, this means that in our consideration, the order of multiperiodicity is defined by the number of different kinds of plasmonic interfaces in U. In the general consideration of multiperiodicity ($U = U^{(a)}U^{(b)}U^{(c)}\ldots$), it is convenient to assume that all different kinds of plasmonic interfaces are contained within the basic cells $U^{(a)}, U^{(b)}, U^{(c)}\ldots$, not caring about appearance of additional kinds of interfaces between the unit cells. That is why we will restrict ourselves with such compositions of $U^{(a)}$ and $U^{(b)}$ where one of the materials is shared, i.e., the biperiodic structure is composed of either one metal and two

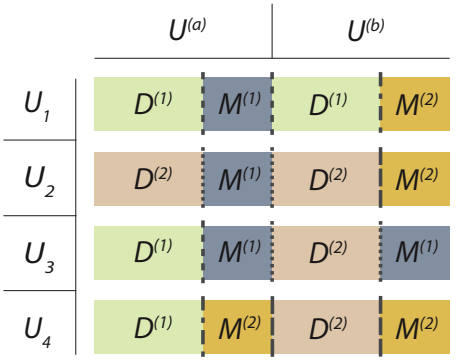

FIG. 2. (Color online) List of generative U's. Different kinds of plasmonic interfaces are highlighted with different dashing.

different dielectrics, or one dielectric and two different metals. The case when U is composed of four entirely different materials will result in more kinds of plasmonic boundaries and does not fall under our definition of multiperiodicity (it is actually a case of biperiodicity with surface plasmons split).

Now, with these restrictions in place, we are able to itemize all possible biperiodic U's. Agreeing for the sake of definiteness that the first layer is dielectric, we come to the following possible basic cells set that define plasmonic interfaces: $U^{(l=a,b)} = \{D^{(1)}M^{(1)}, D^{(1)}M^{(2)}, D^{(2)}M^{(1)}, D^{(2)}M^{(2)}\}$. With this set, four different general plasmonic multilayers can be formed by corresponding generative U's as shown in Fig. 2. It is seen that there are indeed only two sorts of plasmonic interfaces in each U. Therefore, we are indeed dealing with multiperiodicity of the second order, or biperiodicity. In Fig. 1, it is shown how plasmonic interfaces appear in an infinite structure with such unit cells. Our definition of multiperiodicity implies that in the biperiodic case, the interfaces always alternate pairwise, i.e., are sequenced as ... 11221122 ... since each layer is surrounded with the same materials on both sides, bearing in mind that U is repeated infinitely.

In what follows, we will study eigenmodes and corresponding optical properties of mainly, but not exclusively, biperiodic metal-dielectric multilayers arranged according to Fig. 1 with all the possible configurations presented in Fig. 2.

III. TRANSFER MATRICES AND PERMUTATIONS

In order to characterize electromagnetic properties of structures under consideration, let us apply the transfer-matrix formalism to the problem and represent U's as matrices. For a single jth layer of thickness d_j that has permittivity ε_j, the transfer matrix connecting tangential components of electric and magnetic fields is written as follows [25]:

$$M_j = \begin{pmatrix} \kappa_j & -i\frac{\sigma_j}{\xi_j} \\ -i\xi_j\sigma_j & \kappa_j \end{pmatrix}, \quad \begin{aligned} \kappa_j &= \cos\left(k_{x_j}d_j\right), \\ \sigma_j &= \sin\left(k_{x_j}d_j\right). \end{aligned} \tag{1}$$

Throughout this paper, we assume the TM polarization in order to have surface plasmon polaritons at plasmonic interfaces [26]. For this polarization, the term $\xi_j = \varepsilon_j^{-1/2}k_{x_j}/k_j$ is a product of the layer impedance $\varepsilon_j^{-1/2}$ and a ratio where one may recognize the cosine of the propagation angle. For the other (TE) polarization, $\xi_j = \sqrt{\varepsilon_j}k_{x_j}/k_j$. In both cases, $k_j = \sqrt{\varepsilon_j}(\omega/c)$ is the modulus of the wave vector in the layer and $k_{x_j} = \sqrt{k_j^2 - k_y^2}$ is the magnitude of its x component.

In this work, we will consider only real ε_j's, without taking losses into account. Then, it is seen that M_j is a unimodular matrix, i.e., $\det(M_j) = 1$. Unimodularity is a very important property of transfer matrices reflecting the law of conservation of energy.

Knowing the matrix of a single layer, we can now express $U^{(l)}$:

$$\begin{aligned} U^{(l)} &= M_1M_2 \\ &= \begin{pmatrix} \kappa_1\kappa_2 - \frac{\xi_2}{\xi_1}\sigma_1\sigma_2 & -\frac{i}{\xi_1}\sigma_1\kappa_2 - \frac{i}{\xi_2}\kappa_1\sigma_2 \\ -i\xi_1\sigma_1\kappa_2 - i\xi_2\kappa_1\sigma_2 & \kappa_1\kappa_2 - \frac{\xi_1}{\xi_2}\sigma_1\sigma_2 \end{pmatrix}. \end{aligned} \tag{2}$$

Indices 1 and 2 point at the first and the second layer in the cell, respectively. As $U^{(l)}$ is the product of unimodular matrices, it is unimodular as well.

We can express $U^{(l)}$ as a matrix of the form

$$U^{(l)} = \begin{pmatrix} \chi_j \Psi^j & -i\frac{\Phi^j}{\gamma_j} \\ -i\gamma_j \Phi^j & \frac{\Psi^j}{\chi_j} \end{pmatrix}, \tag{3}$$

where $\chi = [1, -\xi_n/\xi_m]$, $\gamma = [\xi_m, \xi_n]$ are coefficients before the vectors Ψ and Φ, defined as

$$\Psi = \begin{bmatrix} \kappa\kappa \\ \sigma\sigma \end{bmatrix}, \quad \Phi = \begin{bmatrix} \sigma\kappa \\ \kappa\sigma \end{bmatrix}, \quad \begin{aligned} \kappa_j &= \cos\left(k_{x_j} d_j\right), \\ \sigma_j &= \sin\left(k_{x_j} d_j\right). \end{aligned} \tag{4}$$

Here, the Einstein summation convention (e.g., $\chi_j \Psi^j = \sum_j \chi_j \Psi^j$) is assumed and will be used throughout the paper. In Eq. (4), the indices at κ and σ are omitted. It is assumed that they coincide with the position of the element in the multiplication string, so that $\kappa\kappa$ means $\kappa_1\kappa_2$ and, for example, $\sigma\kappa$ stands for $\sigma_1\kappa_2$.

If we compare Eqs. (1) and (3), we can realize that recurrence relations can be obtained for the transfer matrix describing the system of $n+1$ layers:

$$\Psi_{n+1} = \begin{bmatrix} \Psi_n \kappa \\ \Phi_n \sigma \end{bmatrix}, \quad \Phi_{n+1} = \begin{bmatrix} \Phi_n \kappa \\ \Psi_n \sigma \end{bmatrix}, \tag{5}$$

$$\chi_{n+1} = \begin{bmatrix} \chi_n & -\frac{\xi_{n+1}}{\gamma_n} \end{bmatrix}, \quad \gamma_{n+1} = \begin{bmatrix} \gamma_n & \frac{\xi_{n+1}}{\chi_n} \end{bmatrix}. \tag{6}$$

With $U^{(l)}$'s determined, it is possible to derive $U = U^{(a)}U^{(b)}$, also a unimodular matrix. Astonishingly, it can be written in the same form as $U^{(l)}$:

$$U = \begin{pmatrix} \chi_j \Psi^j & -i\frac{\Phi^j}{\gamma_j} \\ -i\gamma_j \Phi^j & \frac{\Psi^j}{\chi_j} \end{pmatrix}. \tag{7}$$

Corresponding coefficient columns and permutation rows calculated from (5) and (6) are the following:

$$\chi = \left[1, -\frac{\xi_2}{\xi_1}, -\frac{\xi_3}{\xi_1}, -\frac{\xi_3}{\xi_2}, -\frac{\xi_4}{\xi_1}, -\frac{\xi_4}{\xi_2}, -\frac{\xi_4}{\xi_3}, \frac{\xi_2\xi_4}{\xi_1\xi_3}\right], \tag{8}$$

$$\gamma = \left[\xi_1, \xi_2, \xi_3, -\frac{\xi_1\xi_3}{\xi_2}, \xi_4, -\frac{\xi_1\xi_4}{\xi_2}, -\frac{\xi_1\xi_4}{\xi_3}, -\frac{\xi_2\xi_4}{\xi_3}\right], \tag{9}$$

$$\Psi = \begin{bmatrix} \kappa\kappa\kappa\kappa \\ \sigma\sigma\kappa\kappa \\ \sigma\kappa\sigma\kappa \\ \kappa\sigma\sigma\kappa \\ \sigma\kappa\kappa\sigma \\ \kappa\sigma\kappa\sigma \\ \kappa\kappa\sigma\sigma \\ \sigma\sigma\sigma\sigma \end{bmatrix}, \quad \Phi = \begin{bmatrix} \sigma\kappa\kappa\kappa \\ \kappa\sigma\kappa\kappa \\ \kappa\kappa\sigma\kappa \\ \sigma\sigma\sigma\kappa \\ \kappa\kappa\kappa\sigma \\ \sigma\sigma\kappa\sigma \\ \sigma\kappa\sigma\sigma \\ \kappa\sigma\sigma\sigma \end{bmatrix}. \tag{10}$$

It can be seen that $[\Psi; \Phi]$ contains all the 2^{n-1} permutations of κ and σ of the n layers, and this holds for any multilayer.

Again, we would like to point out that for *arbitrary* multilayer, either periodic or not, the transfer matrix (7) will be of the same form.

IV. DISPERSION EQUATIONS

In order to study the electromagnetic properties of plasmonic multilayers, we shall obtain their dispersion equation from the already derived transfer matrices. Eigenmodes supported by the structure can be found by solving the eigenvalue problem $\det(U - \eta I) = 0$. Keeping in mind that

$$\det(U) = \frac{\chi_j}{\chi_k}\Psi^j\Psi^k + \frac{\gamma_j}{\gamma_k}\Phi^j\Phi^k = 1, \tag{11}$$

we yield the following characteristic polynomial:

$$\eta^2 - \mathrm{tr}(U)\eta + 1, \tag{12}$$

where

$$\mathrm{tr}(U) = \left(\chi_j + \frac{1}{\chi_j}\right)\Psi^j = \mathfrak{x}_j \Psi^j \tag{13}$$

is the trace of U. The roots of the characteristic polynomial are

$$\eta = \frac{\mathfrak{x}_j\Psi^j}{2} \pm i\sqrt{1 - \left(\frac{\mathfrak{x}_j\Psi^j}{2}\right)^2}. \tag{14}$$

For periodic structures having period $\mathfrak{d}$ (see Fig. 1), Bloch's theorem applies in the form $\eta = e^{-ik_x\mathfrak{d}}$, where k_x is the Bloch wave vector of the plasmonic multilayer. For a band of allowed propagating waves, they have real k_x, therefore, $|\eta| = 1$. This leads to an important consequence: the eigenvalues of U are located on the unit circle. From $\mathrm{Re}[\eta]^2 + \mathrm{Im}[\eta]^2 = 1$ it is straightforward to end up with

$$\cos(k_x\mathfrak{d}) = \frac{\mathfrak{x}_j\Psi^j}{2} = \frac{\mathrm{tr}(U)}{2}, \tag{15}$$

which is the dispersion equation sought. Notice that the equation holds for arbitrary periodic multilayer characterized by Ψ, Φ, χ, γ forming U. It is also valid for complex k_x's since Euler's formula applies to complex numbers as well.

If we consider $\omega = 0$, then $k_j = k_{x_j} = k_y = 0$ and we may see that all σ_j's become zero and only the first term in Ψ survives. Since $\chi_1 = 1$, Eq. (15) results in $\cos(k_x\mathfrak{d}) = 1$, which is solved trivially by $k_x = 0$. That is, for any periodic multilayer there is at least one mode that starts from ($\mathbf{k} = 0$, $\omega = 0$).

Now, we write the explicit dispersion expressions for biperiodic plasmonic multilayers. In the case of $U_{1,2}$ configurations with different metals and common dielectric (see Fig. 2), we have

$$\mathfrak{x} = \left[2; -\frac{\xi_d^2 + \xi_{m_1}^2}{\xi_d\xi_{m_1}}; -2; -\frac{\xi_d^2 + \xi_{m_1}^2}{\xi_d\xi_{m_1}}; -\frac{\xi_d^2 + \xi_{m_2}^2}{\xi_d\xi_{m_2}}; -\frac{\xi_{m_1}^2 + \xi_{m_2}^2}{\xi_{m_1}\xi_{m_2}}; -\frac{\xi_d^2 + \xi_{m_2}^2}{\xi_d\xi_{m_2}}; \frac{\xi_d^4 + \xi_{m_1}^2\xi_{m_2}^2}{\xi_d^2\xi_{m_1}\xi_{m_2}}\right], \tag{16}$$

and the dispersion equation reads as follows (the indices m_1,m_2 are omitted in κ,σ combinations in the same manner as above):

$$\begin{aligned}
&2\cos(k_x\mathfrak{d})\\
&=\kappa_d^2(\mathfrak{x}_1\kappa\kappa+\mathfrak{x}_6\sigma\sigma)+\sigma_d^2(\mathfrak{x}_3\kappa\kappa+\mathfrak{x}_8\sigma\sigma)\\
&\quad+\kappa_d\sigma_d\left[(\mathfrak{x}_2+\mathfrak{x}_4)\sigma\kappa+(\mathfrak{x}_5+\mathfrak{x}_7)\kappa\sigma\right]\\
&=\kappa_d^2\left(2\kappa\kappa-\frac{\xi_{m_1}^2+\xi_{m_2}^2}{\xi_{m_1}\xi_{m_2}}\sigma\sigma\right)-\sigma_d^2\left(2\kappa\kappa-\frac{\xi_d^4+\xi_{m_1}^2\xi_{m_2}^2}{\xi_d^2\xi_{m_1}\xi_{m_2}}\sigma\sigma\right)\\
&\quad-2\kappa_d\sigma_d\left[\frac{\xi_d^2+\xi_{m_1}^2}{\xi_d\xi_{m_1}}\sigma\kappa+\frac{\xi_d^2+\xi_{m_2}^2}{\xi_d\xi_{m_2}}\kappa\sigma\right].
\end{aligned}\tag{17}$$

For $U_{3,4}$, i.e., different dielectrics and common metal, the expressions are (now the indices d_1 and d_2 are omitted)

$$\begin{aligned}
\mathfrak{x}=\Bigg[&2;\ -\frac{\xi_m^2+\xi_{d_1}^2}{\xi_m\xi_{d_1}};\ -\frac{\xi_{d_1}^2+\xi_{d_2}^2}{\xi_{d_1}\xi_{d_2}};\ -\frac{\xi_m^2+\xi_{d_2}^2}{\xi_m\xi_{d_2}};\ -\frac{\xi_m^2+\xi_{d_1}^2}{\xi_m\xi_{d_1}};\\
&-2;\ -\frac{\xi_m^2+\xi_{d_2}^2}{\xi_m\xi_{d_2}};\ \frac{\xi_m^4+\xi_{d_1}^2\xi_{d_2}^2}{\xi_m^2\xi_{d_1}\xi_{d_2}}\Bigg],
\end{aligned}\tag{18}$$

$$\begin{aligned}
&2\cos(k_x\mathfrak{d})\\
&=\kappa_m^2(\mathfrak{x}_1\kappa\kappa+\mathfrak{x}_3\sigma\sigma)+\sigma_m^2(\mathfrak{x}_6\kappa\kappa+\mathfrak{x}_8\sigma\sigma)\\
&\quad+\kappa_m\sigma_m\left[(\mathfrak{x}_2+\mathfrak{x}_5)\sigma\kappa+(\mathfrak{x}_4+\mathfrak{x}_7)\kappa\sigma\right]\\
&=\kappa_m^2\left(2\kappa\kappa-\frac{\xi_{d_1}^2+\xi_{d_2}^2}{\xi_{d_1}\xi_{d_2}}\sigma\sigma\right)-\sigma_m^2\left(2\kappa\kappa-\frac{\xi_m^4+\xi_{d_1}^2\xi_{d_2}^2}{\xi_m^2\xi_{d_1}\xi_{d_2}}\sigma\sigma\right)\\
&\quad-2\kappa_m\sigma_m\left[\frac{\xi_m^2+\xi_{d_1}^2}{\xi_m\xi_{d_1}}\sigma\kappa+\frac{\xi_m^2+\xi_{d_2}^2}{\xi_m\xi_{d_2}}\kappa\sigma\right].
\end{aligned}\tag{19}$$

Transition between Eqs. (17) and (19) can be made if index transformations $d\leftrightarrow m$ and $m_1,m_2\leftrightarrow d_1,d_2$ are applied. The equations become equivalent if we assume both equal dielectrics and equal metals, i.e., a common periodic metal-dielectric multilayer. In this case,

$$\begin{aligned}
\mathrm{tr}(U^{(l)}U^{(l)})&=4\kappa_d^2\kappa_m^2-4\left(\frac{\xi_d}{\xi_m}+\frac{\xi_m}{\xi_d}\right)\kappa_d\kappa_m\sigma_d\sigma_m\\
&\quad+\left(\frac{\xi_d^2}{\xi_m^2}+\frac{\xi_m^2}{\xi_d^2}\right)\sigma_d^2\sigma_m^2+2\sigma_d^2\sigma_m^2\\
&=\left[2\kappa_d\kappa_m-\left(\frac{\xi_d}{\xi_m}+\frac{\xi_m}{\xi_d}\right)\sigma_d\sigma_m\right]^2=\mathrm{tr}^2(U^{(l)}),
\end{aligned}\tag{20}$$

exactly as it is expected from matrix algebra since the eigenvalues of a matrix squared is equal to squares of its eigenvalues.

V. QUASISTATIC AND LONG-WAVELENGTH LIMIT

In the quasistatic limit, when ω comes close to zero, $k_j(\omega)$ tends to zero too and it is obvious that $k_j\sim k_{x_j}\sim k_y\to 0$. Using the O notation, one may write for finite C that $O(Cf(\omega))=O(f(\omega))$. In the case of ε_d being the permittivity of a dielectric that is constant $O(\varepsilon_d f(\omega))=O(f(\omega))$, i.e., product of the infinitesimal and a finite constant is infinitesimal as well. Therefore, $k_d=\sqrt{\varepsilon_d}(\omega/c)=O(\omega)$. In the case of a metal, the problem is a little more complicated since the Drude formula goes to infinity as ω reaches zero: $\varepsilon_m=\varepsilon_m(\omega^{-2})$. Nevertheless, $k_m=\sqrt{\varepsilon_m(\omega^{-2})}(\omega/c)=iC$ which means ε_m only lessens the order of the infinitesimal function k_m and does not introduce any singularity in it. In reality, however, permittivity of metals is almost entirely imaginary valued at low frequencies. As we do not account for losses in this work, ε_m will be considered as a finite negative constant in the quasistatic approximation assuming that $k_j=O(\omega)$ both for dielectric and metal layers. Now, let us define α as the following set of functions: $\alpha=C_1^2[C_2(\omega/c)^2-k_y^2]=O(f(\omega^2,k_y^2))$, with $C_1,C_2\in\mathbb{R}$ being some constants. Thus, we can express κ_j,σ_j in the quasistatic limit:

$$\begin{aligned}
\kappa_j&\to 1-\frac{d_j^2}{2}\left(k_j^2-k_y^2\right)+\frac{d_j^2}{4!}\left(k_j^2-k_y^2\right)^2=1-\alpha+\alpha^2,\\
\sigma_j&\to d_j\left(k_j^2-k_y^2\right)^{1/2}-\frac{d_j^3}{3!}\left(k_j^2-k_y^2\right)^{3/2}=\alpha^{1/2}-\alpha^{3/2},
\end{aligned}\tag{21}$$

where the order of expansion is determined solely by the last term in Ψ. In our case, we should take into account terms up to α^2 so that this term remains nonvanishing. Thus, this is what remains in Ψ (repeating terms are skipped):

$$\Psi=\begin{bmatrix}10\alpha^2-4\alpha+1\\-4\alpha^2+\alpha\\\dots\\-4\alpha^2+\alpha\\\alpha^2\end{bmatrix}.\tag{22}$$

Next, we clarify what happens to $\mathfrak{x}$. For ξ_j there is the following limit:

$$\xi_j\to\frac{1}{\sqrt{\varepsilon_j}}\sqrt{1-\frac{k_y^2}{k_j^2}}\to 0.\tag{23}$$

The only quantities that enter χ are of the kind ξ_i/ξ_j. Let us suppose these quantities equal unity in the sense that they all share the same order of infinitesimals, i.e., $\xi_i=O(\xi_j)$ and $\xi_j=O(\xi_i)$ simultaneously. However, we should keep in mind that in $\mathfrak{x}$ they are summed with their inverses, leading to the appearance of quadratic terms. Since $\varepsilon_m<0$, for metals $\xi_j^2\to-0$, while in the case of dielectrics $\xi_j^2\to+0$. Taking this fact into account, we obtain thereby (repeating terms are skipped)

$$\mathfrak{x}=[2\ \dots\ 2].\tag{24}$$

Considering propagation along the layers, i.e., with $k_x=0$, Eq. (15) gives

$$-13\alpha^2+2\alpha=0.\tag{25}$$

From Sec. IV we already know that a trivial solution always exists for a multilayer, meaning that lower modes start from zero frequency. Equation (25) has two solutions, with $\alpha=0$ approaching the light line. As a result, $\alpha=\{0,\alpha_1\}$ states that there are two lower eigenmodes in the biperiodic plasmonic multilayer, one corresponding to the light line and the other deviating from it. Moreover, it can be seen by induction that an overall number of low-frequency modes is equal

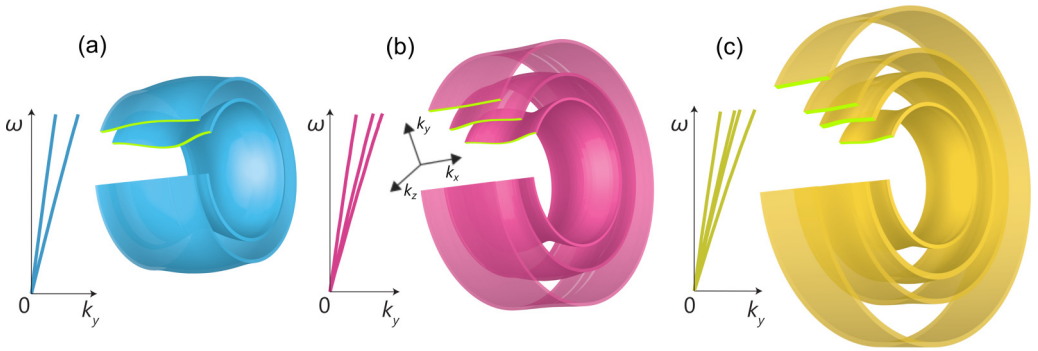

FIG. 3. (Color online) Asymptotic dispersion diagrams and isofrequency surfaces (in arbitrary units) typical for plasmonic multilayers in the long-wavelength limit. Structures are designed to embody the multiperiodicity of (a) the second order (bi-periodicity), (b) the third order, and (c) the fourth order. Cross sections of the surfaces (the isofrequency contours) are marked with green.

to the number of different kinds of plasmonic interfaces in the unit cell defining the order of multiperiodicity. Namely, $\alpha = \{0,\alpha_1,\ldots,\alpha_{n-1}\}$. Attention should be paid to the fact that this result does not rely upon a specific configuration of U. Additional modes are observed for arbitrary multiperiodic multilayers with unit cells having n different plasmonic interfaces. Kindred multiband behavior may also be observed in a class of three-dimensional hybridized metamaterials [27].

Isofrequency surfaces $k_x(k_y,k_z)$ for low-frequency modes of plasmonic multilayers in the cases of $n = 2,3,4$ are demonstrated in Fig. 3. Biperiodicity assumes the presence of two modes in the long-wavelength limit, exactly as Fig. 3(a) shows. The inner surface is of the shape of a wheel rim, which corresponds to the hyperbolic isofrequency contour. The outward surface is rather flat and has an inverted camber profile. For higher-order multiperiodic multilayers, additional high-k surfaces are added in addition to these two ones, getting flatter and flatter with the increase of n. Each increase of n adds a new disconnected surface. Such a diversity of topologies seen in isofrequency surfaces arises due to the plasmonic nature of the structures considered in this work. All-dielectric multilayers would always have an ellipsoid as the isofrequency surface at low frequencies, without additional modes.

Note that one can also view the increasing number of isofrequency surfaces in Fig. 3 as the mode structure of an array of weakly coupled dielectric waveguides sandwiched between perfect electrically conducting walls since one can notice that the Drude model becomes similar to the perfect electric conductor in the long-wavelength limit.

We would also like to reiterate that in the case of equal metals and dielectrics, the structure is identical to the plasmonic multilayer composed of two alternating layers. Additional modes are arising due to the appearance of solutions corresponding to $k_x = 2\pi/(\mathfrak{n}\mathfrak{d}),\mathfrak{n} = 2\ldots n$, in such consideration of two-layered cells.

Another approach to the long-wavelength regime is to make the thickness of the unit cell $\mathfrak{d}$ approaches zero. It is usually assumed that when the wavelength is much larger then the thickness of the period, the local effective-medium theory can be used. Such an approximation can be applied to multiperiodic multilayers in the same manner as to the basic periodic case with only one kind of plasmonic interface, so we introduce it here for completeness.

As a general rule, the local effective-medium theory assumes that the fields do not vary in the layers and are constant. Since the tangential component of the electric field should be conserved, we are able to write the effective-medium permittivity tensor in the case of n arbitrary layers, alternating periodically in the multilayer:

$$\hat{\varepsilon}_{ij}^{\text{eff}} = \begin{vmatrix} \varepsilon_{\parallel}^{\text{eff}}\delta_{ij}, & i,j = 1,2 \\ \varepsilon_{\perp}^{\text{eff}}\delta_{ij}, & i,j = 3 \end{vmatrix} \tag{26}$$

$$\varepsilon_{\parallel}^{\text{eff}} = \frac{\sum_n \varepsilon_n d_n}{\sum_n d_n}, \quad \varepsilon_{\perp}^{\text{eff}} = \left(\frac{\sum_n \varepsilon_n^{-1} d_n}{\sum_n d_n}\right)^{-1}. \tag{27}$$

In the case of, e.g., different dielectrics and common metal, we obtain

$$\varepsilon_{\parallel}^{\text{eff}} = \frac{1}{2}\frac{(\varepsilon_{d_1} + \varepsilon_{d_2})d_d}{D} + \frac{\varepsilon_m d_m}{D}, \tag{28}$$

$$\varepsilon_{\perp}^{\text{eff}} = 2\left(\frac{(\varepsilon_{d_1}^{-1} + \varepsilon_{d_2}^{-1})d_d + 2\varepsilon_m^{-1} d_m}{D}\right)^{-1}, \tag{29}$$

where $\varepsilon_{d_1},\varepsilon_{d_2}$ are permittivities of different dielectrics and ε_m is a permittivity of the common metal. Once again, for different metals it is only needed to interchange the indices d and m coming to $\varepsilon_{m_1},\varepsilon_{m_2}$ as permittivities for different metals.

One should pay attention that the local effective-medium approximation typically fails to describe electromagnetic response of plasmonic multilayers in presence of strong variation of the field inside the layers. However, it may be useful in some cases, as will be shown in the following.

VI. PHOTONIC BAND STRUCTURE

The dispersion equations obtained in the previous sections allow us to study photonic band structures and optical properties of multiperiodic plasmonic multilayers semianalytically. In this section, we consider in detail the case of biperiodicity shown in Figs. 1 and 2. Namely, we remind that the structure is formed using two different plasmonic interfaces defined by $U^{(a)}$ and $U^{(b)}$, each consisting of a dielectric layer and a metal layer. Permittivities of dielectrics are taken to be constant, while for metal layers the Drude model is assumed. For the

$U_{1,2}$ configurations, the plasma frequencies of metals ω_{p1} and ω_{p2} are slightly detuned from each other, and we put $\omega_{p1} < \omega_{p2}$. All dielectric layers have thickness d_d and metal layers have thickness d_m; the total thickness of the unit cell is $\mathfrak{d} = 2(d_d + d_m)$.

Since there are two different plasmonic interfaces in the unit cell, there are two resonant frequencies $\omega_{sp1,sp2}$ defined as

$$\begin{aligned} U_{1,2} &: \omega_{sp1,sp2} = \frac{\omega_{p1,p2}}{\sqrt{1+\varepsilon_d}}, \\ U_{3,4} &: \omega_{sp1,sp2} = \frac{\omega_p}{\sqrt{1+\varepsilon_{d1,d2}}}, \end{aligned} \tag{30}$$

at which the dielectric and metal permittivites are opposite, and surface plasmons are excited:

$$\begin{aligned} U_{1,2} &: \varepsilon_{m1}(\omega_{sp1}) = -\varepsilon_d, \quad \varepsilon_{m2}(\omega_{sp2}) = -\varepsilon_d; \\ U_{3,4} &: \varepsilon_m(\omega_{sp1}) = -\varepsilon_{d1}, \quad \varepsilon_m(\omega_{sp2}) = -\varepsilon_{d2}. \end{aligned} \tag{31}$$

Given the existence of two surface plasmon frequencies, it is natural to introduce the normalized frequency $\tilde{W}$, which is zero at the first resonance and unity at the second one. The expression for $\tilde{W}$ is thus

$$\tilde{W} = \frac{\omega - \omega_{sp1}}{\omega_{sp2} - \omega_{sp1}}. \tag{32}$$

Figures 4 and 5 show the photonic band structure of plasmonic multilayers calculated from (17) and (19). As was demonstrated previously [11,28], two dispersion branches are present in the plasmonic multilayer formed by $U^{(l)}$. When the multilayer is formed by the four-layered unit cell

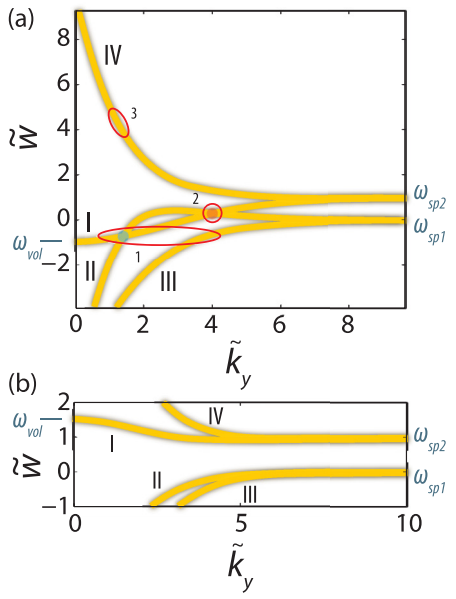

FIG. 4. (Color online) Band diagrams showing k_x zero eigenwaves of the plasmonic multilayer in (a) $U_{1<}$ and (b) $U_{1>}$ configurations, as per Eq. (35). Frequency is normalized according to Eq. (32), and wave numbers are normalized by a factor of $\pi/\mathfrak{d}$. Roman numerals (I–IV) number the modes; highlighted regions numbered as 1–3 correspond to characteristic cases depicted in Fig. 6. Blue and red dots denote mode crossings.

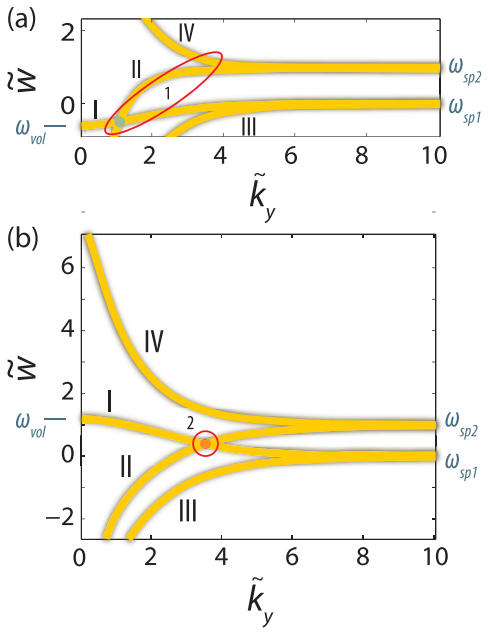

FIG. 5. (Color online) Band diagrams for the plasmonic multilayer in (a) $U_{3<}$ and (b) $U_{3>}$ configurations, as per Eq. (36). Highlighted regions 1 and 2 correspond to characteristic cases shown in Fig. 7. The rest is the same as in Fig. 4

$U = U^{(a)}U^{(b)}$, two additional modes appear, resulting in four branches in total. Generally, the appearance of additional modes is not surprising, as it can be expected, for example, from the analysis of multilayered waveguides [29,30]. Also, four distinct waves in the optical domain were reported in five-layered structures with only one plasmonic interface [31,32], which are therefore not genuinely multiperiodic in terms of our definition.

In the region 1 of Figs. 4(a) and 5(a), we see that the mode I emerges from the ordinate axis at the frequency ω_{vol}, which corresponds to the volume plasmon. We also see that the modes I and II cross near that frequency. In the effective-medium limit ($\mathfrak{d} \to 0$), we can yield an expression for ω_{vol} because in that limit, $\varepsilon_{\parallel}^{\text{eff}}(\omega_{\text{vol}}) = 0$ by definition. The resulting expressions for ω_{vol} can then be written for different configurations:

$$U_{1,2}: \ \omega_{\text{vol}} = \sqrt{\frac{\omega_{p1}^2 + \omega_{p2}^2}{2\left(1+\varepsilon_d \frac{d_d}{d_m}\right)}} = \sqrt{\frac{\langle \omega_p^2 \rangle}{1+\varepsilon_d \frac{d_d}{d_m}}}, \tag{33}$$

$$U_{3,4}: \ \omega_{\text{vol}} = \sqrt{\frac{\omega_{pi}^2}{1+\frac{1}{2}(\varepsilon_{d1}+\varepsilon_{d2})\frac{d_d}{d_m}}} = \sqrt{\frac{\omega_{pi}^2}{1+\langle \varepsilon_d \rangle \frac{d_d}{d_m}}}. \tag{34}$$

Both expressions contain averaged values: the mean of the squared plasma frequencies for $U_{1,2}$ and average permittivity of dielectrics for $U_{3,4}$. That is, ω_{vol} in bi-periodic plasmonic multilayers is none other than the averaging of volume plasmon frequencies of the constitutive systems $U^{(l)}$. Equations (33) and (34) can be obtained from Eqs. (17) and (19) by expanding the latter over the layer thicknesses, taking into account terms up to the second order. One may obtain more precise expressions for ω_{vol} if the terms up to the fourth order are kept.

Whether or not the modes I and II cross near $\omega_{\rm vol}$ is determined by the frequency of the volume plasmon relative to that of the surface plasmons, which can be learned from Figs. 4(a) and 5(a). For the mode crossing to take place, the volume plasmon should be below both surface plasmons, i.e., $\omega_{\rm vol} \leq \min(\omega_{sp1},\omega_{sp2})$ and mode I emerges below surface plasmons. Taking into account our previous assumption $\omega_{p1} < \omega_{p2}$, the crossing condition is fulfilled in $U_{1,2}$ configurations when

$$\frac{d_d}{d_m} > \frac{1}{2}\left[1+\frac{\omega_{p2}^2}{\omega_{p1}^2}-\frac{1}{\varepsilon_d}\left(1-\frac{\omega_{p2}^2}{\omega_{p1}^2}\right)\right]. \tag{35}$$

The corresponding expressions for the $U_{3,4}$ configurations, given the previous assumption $\varepsilon_{d1} < \varepsilon_{d2}$, are

$$\frac{d_d}{d_m} > 2\frac{\varepsilon_{d1}}{\varepsilon_{d1}+\varepsilon_{d2}}. \tag{36}$$

Equations (35) and (36) act as criteria for the thicknesses of metal and dielectric layers as regards their influence on the band structure. In what follows, we will denote thinner-metal multilayers meeting these criteria with the subscript "<" and the remaining (thicker-metal) multilayers with the subscript ">." Figures 4 and 5 confirm that these two cases give rise to topologically distinct band diagrams.

Both (35) and (36) are valid under the effective-medium approach, so a rather good prediction for the mode crossing point is only achieved when $\mathfrak{d} \to 0$. The thinner the full period, and the further $\omega_{\rm vol}$ deviates from $\omega_{sp1,sp2}$, the better the effective-medium approximates the volume plasmon frequencies.

Figures 6 and 7 show three-dimensional dispersion surfaces $\tilde{W}(k_x,k_y)$ for some characteristic cases of Figs. 4 and 5, respectively. For the regions labeled as "1," i.e., the crossing of modes I and II, we see [Figs. 6(1) and 7(1)] that the crossing appears as touching of the inner contours, a hyperbolic and

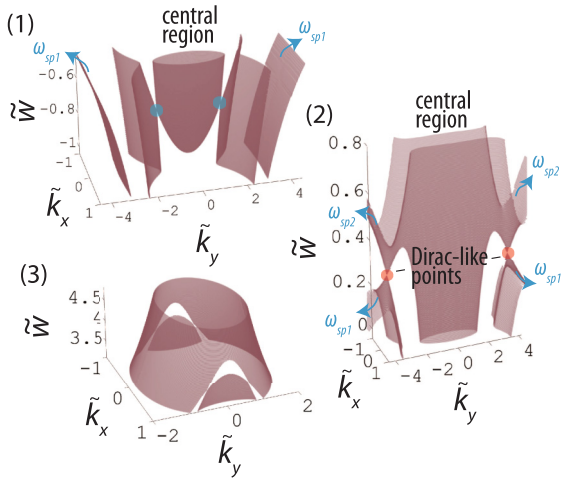

FIG. 6. (Color online) Dispersion surfaces corresponding to regions 1–3 of Fig. 4, with k_x spanning the first Brillouin zone. Blue arrows mark the asymptotic behavior of the dispersion surfaces as $\tilde{k}_y \to \infty$, tending towards $\tilde{W} = 0$ or 1. Blue dots indicate touching points between the surfaces at the crossing between modes I and II [see Fig. 4(a)]. Red dots indicate Dirac-type points, where outer dispersion surfaces collapse.

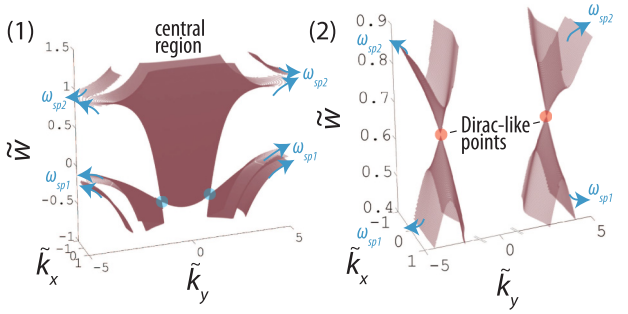

FIG. 7. (Color online) Dispersion surfaces corresponding to regions 1 and 2 of band diagrams of Fig. 5. Red dots indicate *isolated* Dirac-type points. The rest is the same as in Fig. 6.

an elliptic one, which is highlighted in the figures. The first surface plasmon frequency ω_{sp1} (or $\tilde{W} = 0$), lying above the frequency of the crossing point between modes I and II, serves as an asymptote for two of the four modes (I and III or II and III, depending on the configuration) as $\tilde{k}_y \to \infty$, indicated in Figs. 6(1) and 7(1) with blue arrows. Close to ω_{sp1}, various eigenmodes behave in a rather different fashion for each specific configuration, as described in Table I, but in all the cases the mode III cuts off at $\tilde{W} = 0$.

In the lower half of Figs. 6(2) and 7(2) showing region 2 in Figs. 4 and 5, respectively, we observe how the outer contours behave past the first resonance, i.e., for $\tilde{W} > 0$. We see that there are several special points where the contours collapse [as can be seen from, e.g., Fig. 7(2)]. From the analysis of the band structure we learn that this occurs near a certain frequency $\omega_{\rm col}$ between those for the two surface plasmons: $\omega_{sp1} < \omega_{\rm col} < \omega_{sp2}$. It is determined by

$$\omega_{\rm col} = \frac{\omega_{p1,p2}}{\sqrt{1+\langle\varepsilon_d\rangle}}. \tag{37}$$

Around this $\omega_{\rm col}$, the dispersion surfaces become cone shaped.

We also notice that the central region of the Brillouin zone contains a dispersion surface at the frequencies between surface plasmons in $U_<$ configurations, but is devoid of bands in the case of $U_>$. In Fig. 4(b), this absence of modes in the center of the Brillouin zone leads to a band gap in frequency. In contrast to the case of $U_{3<,4<}$, the conelike outer bands in the dispersion surface form isolated nontrivial *Dirac-type cones*, as seen in Fig. 8(a). The points corresponding to the intersection of these cones at $\omega_{\rm col}$ are therefore called the Dirac-type points. Their exact location would vary slightly with the change of the layer thicknesses. Conventionally, such

TABLE I. Behavior of the photonic bands nearby $\tilde{W} = 0$.

	$U_<$	$U_>$
$U_{1,2}$	Modes I and II form an elliptic and a hyperbolic band.	Mode II cuts off at ω_{sp1}. Band gap is present above the surface plasmon.
$U_{3,4}$	Mode I cuts off at ω_{sp1}. Mode II forms an elliptic band in the central region.	Mode II forms a hyperbolic band. No modes are in the center of the Brillouin zone.

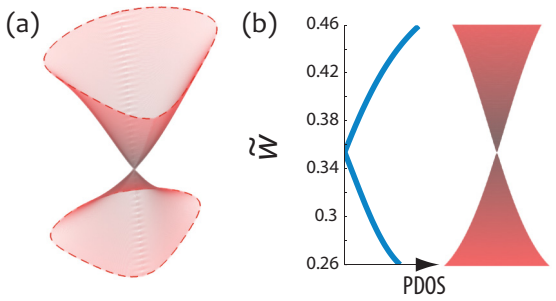

FIG. 8. (Color online) (a) An enlarged view of an isolated Dirac-type cone of Fig. 7(2), with its cross section marked by the dashed line. (b) Zero photon density of states corresponding to the Dirac-type point (in arbitrary units).

Dirac points occur in the center of the Brillouin zone where $\mathbf{k} = 0$, as it takes place in numerous photonic analogs of the Dirac cones observed in graphene [33–35] or, alternatively, Dirac cones may be observed at the corners of the Brillouin zone [36]. Here, we have, however, nontrivial high-k Dirac states far away from the center of the zone. Moreover, the cones are pinned to each other in a robust way and do not get disconnected for arbitrary filling ratios in $U_{3<,4<}$ configurations. We point out once again that isolated Dirac points (without an accompanying band in the center of the Brillouin zone) are only present in the case of $U_{3,4}$ (same metal, different dielectrics).

At these Dirac points, the structure changes from all-negatively to all-positively refracting. A number of effects are associated with the Dirac points in metamaterials, such as *Zitterbewegung* of optical pulses [37–39], field localization and enhancement [40], and giant optical nonlocality [41]. One of the main characteristics of these points is that they are states with zero photonic density of states (PDOS). For the mth mode, PDOS is proportional to $\int d^2\mathbf{k}\,\delta(\omega - \omega_m(\mathbf{k}))$ and is fully defined by dispersion surfaces. When these collapse into a set of points, PDOS becomes zero. It can be seen in Fig. 8(b), where it is also demonstrated that PDOS is almost symmetrical around the Dirac point.

Above the Dirac points frequency we can see the second surface plasmon at $\tilde{W} = 1$, where there are outer dispersion branches tending to ω_{sp2} asymptotically. Finally, for frequencies higher than the second surface plasmon resonance ($\tilde{W} > 1$), a bottleneck-shaped surface is seen to appear in the dispersion relations [see Fig. 6(3)]. In all the band diagrams showing eigenmode structures for different U's it corresponds to the broadband backward-propagating mode IV. This mode is also of special interest, as it realizes broadband negative refraction up to the ultraviolet region [10].

VII. CONCLUSIONS

We have defined multiperiodicity in plasmonic multilayers and introduced the permutation-based formalism for its universal description within the transfer-matrix approach. It was shown that for an arbitrary multilayer, its transfer matrix can be written in the same form differing only in permutation vectors and corresponding coefficient rows. Low-frequency modes of plasmonic multilayers have been analyzed, and it was shown that their number is equal to the order of multiperiodicity. Multiperiodicity up to the fourth order has been considered. We have shown the formation of diverse topological structures in isofrequency and dispersion surfaces. Relations between the topological features of these surfaces and geometrical configuration of the biperiodic multilayers have been established and explained using the interplay between surface plasmon polaritons at individual metal-dielectric interfaces and volume plasmon polaritons in the effective-medium limit. For some biperiodic configurations, namely, those with two different kinds of dielectrics and one kind of metal ($U_{3,4}$ as shown in Fig. 2), vanishing photonic density of states and isolated nontrivial Dirac cones have been observed, differing from the conventional Dirac cones in photonic structure by their high-k location in the wave-vector space.

ACKNOWLEDGMENTS

This work was supported by the Ministry of Education and Science of the Russian Federation (Project No. 11.G34.31.0020), the President of Russian Federation (Grant No. SP-2154.2012.1), and the Government of Russian Federation (Grant No. 074-U01). S.V.Z. wishes to acknowledge financial support from the People Programme (Marie Curie Actions) of the European Union's 7th Framework Programme FP7-PEOPLE-2011-IIF under REA Grant Agreement No. 302009 (Project HyPHONE).

[1] Lord Rayleigh, Proc. R. Soc. London, Ser. A **93**, 577 (1917).
[2] L. Brillouin, *Wave Propagation in Periodic Structures* (McGraw-Hill, New York, 1946).
[3] L. Brillouin and M. Parodi, *Propagation of Waves in Periodic Media* (Dunod, Paris, 1956).
[4] L. M. Brekhovskikh, *Waves in Layered Media* (Academic, New York, 1960).
[5] H. N. S. Krishnamoorthy, Z. Jacob, E. Narimanov, I. Kretzschmar, and V. M. Menon, Science **336**, 205 (2012).
[6] J. Luo, H. Chen, B. Hou, P. Xu, and Y. Lai, Plasmonics **8**, 1095 (2013).
[7] K. L. Tsakmakidis, A. D. Boardman, and O. Hess, Nature (London) **450**, 397 (2007).
[8] A. A. Orlov, S. V. Zhukovsky, I. V. Iorsh, and P. A. Belov, Phot. Nanostr. Fund. Appl. **12**, 213 (2014).
[9] E. Verhagen, Rene de Waele, L. Kuipers, and A. Polman, Phys. Rev. Lett. **105**, 223901 (2010).
[10] T. Xu, A. Agrawal, M. Abashin, K. J. Chau, and H. J. Lezec, Nature (London) **497**, 470 (2013).
[11] A. A. Orlov, P. M. Voroshilov, P. A. Belov, and Yu. S. Kivshar, Phys. Rev. B **84**, 045424 (2011).
[12] G. Castaldi, V. Galdi, A. Alù, and N. Engheta, Phys. Rev. Lett. **108**, 063902 (2012).

[13] A. V. Chebykin, A. A. Orlov, C. R. Simovski, Y. S. Kivshar, and P. A. Belov, Phys. Rev. B **86**, 115420 (2012).
[14] Z. Jacob, I. I. Smolyaninov, and E. E. Narimanov, Appl. Phys. Lett. **100**, 181105 (2012).
[15] I. Iorsh, A. Poddubny, A. Orlov, P. Belov, and Y. S. Kivshar, Phys. Lett. A **376**, 185 (2012).
[16] J. Elser, A. A. Govyadinov, I. Avrutsky, I. Salakhutdinov, and V. A. Podolskiy, J. Nanomater. **2007**, 79469 (2007).
[17] W. Yan, M. Wubs, and N. A. Mortensen, Phys. Rev. B **86**, 205429 (2012).
[18] T. U. Tumkur, Lei Gu, J. K. Kitur, E. E. Narimanov, and M. A. Noginov, Appl. Phys. Lett. **100**, 161103 (2012).
[19] R. Maas, J. Parsons, N. Engheta, and A. Polman, Nat. Photonics **7**, 907 (2013).
[20] O. Kidwai, S. V. Zhukovsky, and J. E. Sipe, Phys. Rev. A **85**, 053842 (2012).
[21] S. V. Zhukovsky, O. Kidwai, and J. E. Sipe, Opt. Express **21**, 14982 (2013).
[22] A. V. Chebykin, A. A. Orlov, A. V. Vozianova, S. I. Maslovski, Y. S. Kivshar, and P. A. Belov, Phys. Rev. B **84**, 115438 (2011).
[23] S. V. Zhukovsky, A. V. Lavrinenko, and J. E. Sipe, in *Proceedings of SPIE, Ottawa, Canada, June 2013* (SPIE, Bellinghan, WA, 2013), Vol. 8915, p. 891512.
[24] E. E. Narimanov, arXiv:1402.0681.
[25] M. Born and E. Wolf, *Principles of Optics: Electromagnetic Theory of Propagation, Interference and Diffraction of Light* (Pergamon, Oxford, 1964).
[26] S. A. Maier, *Plasmonics: Fundamentals and Applications* (Springer, Berlin, 2007).
[27] J. Shin, J.-T. Shen, and S. Fan, Phys. Rev. B **76**, 113101 (2007).
[28] R. J. Pollard, A. Murphy, W. R. Hendren, P. R. Evans, R. Atkinson, G. A. Wurtz, A. V. Zayats, and V. A. Podolskiy, Phys. Rev. Lett. **102**, 127405 (2009).
[29] Ş. E. Kocabaş, G. Veronis, D. A. B. Miller, and S. Fan, Phys. Rev. B **79**, 035120 (2009).
[30] I. Avrutsky, I. Salakhutdinov, J. Elser, and V. Podolskiy, Phys. Rev. B **75**, 241402 (2007).
[31] H. Alaeian and J. A. Dionne, Phys. Rev. B **89**, 075136 (2014).
[32] H. Alaeian and J. A. Dionne, Phys. Rev. A **89**, 033829 (2014).
[33] X. Huang, Y. Lai, Z. H. Hang, H. Zheng, and C. T. Chan, Nat. Mater. **10**, 582 (2011).
[34] K. Sakoda, Opt. Express **20**, 3898 (2012).
[35] K. Sakoda, Opt. Express **20**, 9925 (2012).
[36] O. Peleg, G. Bartal, B. Freedman, O. Manela, M. Segev, and D. N. Christodoulides, Phys. Rev. Lett. **98**, 103901 (2007).
[37] X. Zhang, Phys. Rev. Lett. **100**, 113903 (2008).
[38] L.-G. Wang, Z.-G. Wang, and S.-Y. Zhu, Europhys. Lett. **86**, 47008 (2009).
[39] X. Ling, Z. Tang, and L. Chen, Opt. Commun. **321**, 96 (2014).
[40] G. D'Aguanno, N. Mattiucci, C. Conti, and M. J. Bloemer, Phys. Rev. B **87**, 085135 (2013).
[41] L. Sun, J. Gao, and X. Yang, Opt. Express **21**, 21542 (2013).